MAGNETIC BUBBLE MEMORY

Magnetic bubble and Bloch line memories, similar to other types of magnetic memories (disk, tape, core), store information by creating a specific magnetic structure that is read by appropriate sensors. In a bubble memory, a cylindrical magnetic domain (called a *magnetic bubble*) represents the unit of information storage. The magnetic bubble resides in a thin magnetic film whose magnetization is perpendicular to the plane of the film. The bubble is magnetized in the direction opposite to the magnetization of the surrounding region.

Proposed Bloch line memories store information in the magnetic structure of the domain wall, the region separating two oppositely magnetized domains. The reading and writing of binary information in Bloch line memories employs bubble memory technology.

Magnetic bubble and Bloch line memories are solid-state magnetic memories. There are no moving parts. The domains are moved to the detector through the actions of magnetic fields. In contrast, other forms of magnetic memory, such as tape and disk drives, feature the physical movement of the magnetic domain to a read head.

HISTORY

Kooy and Enz (1) observed cylindrical magnetic domains in barium ferrite ($BaFe_{12}O_{19}$) platelets. Bobeck (2) described the properties of cylindrical magnetic domains in orthoferrite platelets with uniaxial magnetic anisotropy. Bobeck's paper alluded to the possibility of using the cylindrical domains for information storage. The technical community became very interested in magnetic bubbles after Bobeck showed a 12-minute movie at the 1969 Intermag (International Magnetics) conference which demonstrated a shift-register storage device in which the bubble was the unit of information storage (3). US Patent 3,460,116 in 1969 described the Magnetic Domain Propagation Circuit invented by A. H. Bobeck, U. F. Gianola, R. C. Sherwood and W. Shockley.

Within a decade of Bobeck's article, several bubble memory products had arrived in the marketplace (3). Hitachi announced a 32 kbyte memory unit, consisting of sixteen 16-kbit chips, for $667 in October 1975. Similar products were announced by Rockwell International and Plessey shortly afterwards. Texas Instruments introduced a 92 kbit memory module. NASA, with Rockwell, announced a 10^8 bit bubble data recorder. Increases in the capacity of bubble memory were rapid. In the early 1980s Intel offered the 7110 and 7114 bubble memory packages with capacities of 1 Mbit and 4 Mbit, respectively. (An Intel Bubble Memory prototype board is shown in Fig. 1.) Similar products were available from Hitachi Corporation. In spite of innovative proposals (3) to increase the density, the rapid increase in capacity of the early years of bubble memory did not continue. Most manufacturers of bubble memory left the market. As of the late 1990s, as

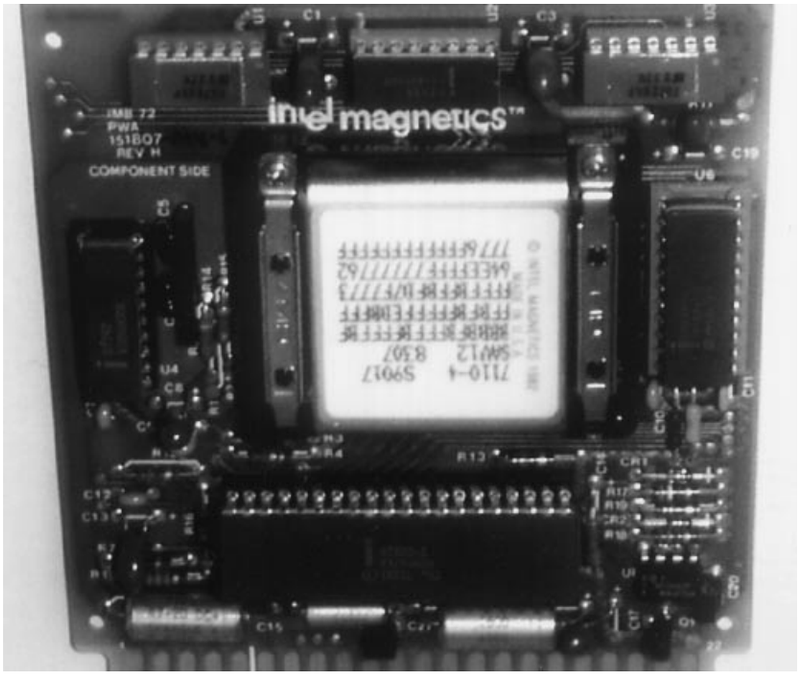

Figure 1. Intel bubble memory prototype board. The large package is the 7110 magnetic bubble circuit. The smaller integrated circuits are for support functions, including generating the current for the rotating magnetic field and for reading and writing. Photo by J. Woodall.

far as the authors know, Sagem in France is the only producer of magnetic bubble memory.

Magnetic bubble memory was intended to bridge the cost/access gap between high-cost and high-speed semiconductor RAM and low-cost and low-speed magnetic tape. Compared to volatile semiconductor RAM, bubble memory is nonvolatile and radiation hard, desirable features for aerospace applications. Because a bubble memory has no moving parts, some supporters perceived a potential advantage over mechanical disk drives. However, because of technological improvements, mechanical disk drives soon proved to have a lower cost per unit of information storage than could be achieved with bubble memory. Cost drawbacks of bubble memory included a relatively bulky package with a permanent magnet to maintain the magnetic state of the bubbles and driver coils to move the bubbles. Another cost drawback was the price of the single-crystal, gadolinium gallium garnet substrate and thin epitaxial magnetic film materials used in fabrication. Further contributing to the noncompetitive cost of bubble memories was small operating margins with the resulting unfavorable yield.

The domain wall, the magnetic boundary between the inside and outside of the cylindrical magnetic domain, is an important factor in magnetic bubble memory. Early on, it was realized that there may be magnetic twists in the domain wall (4), known as Bloch lines. A Bloch line that extends through the thickness of the film is known as a vertical Bloch line (VBL). It was shown by Malozemoff and Slonczewski (5) that the generation of Bloch lines places a limit on the maximum speed of a magnetic bubble. The bubble speed limits the access time, the time required to bring a bubble from its storage location on the chip to the detector. A bubble with a great number of Bloch lines is known as a hard bubble, which is difficult to move because of its low mobility and would result in a memory error. Ion implantation was found to be an effective method for suppressing hard bubbles.

In 1983, S. Konishi of Kyushi University, proposed a concept for dramatically increasing the storage density in a magnetic garnet film (6). The unit of information storage was to be the vertical Bloch line. Because a single bubble can have in excess of 100 VBLs in its wall, now there was the potential for a significant increase in the areal density of solid-state magnetic storage. Konishi projected a possible density of 1.6 Gbit/cm^2, which was a remarkable density at the time. Researchers at several institutions, including Hitachi, Kyushu University, NEC, Sony, and University of Electro-Communications in Japan, LETI and Sagem in France, the University of Wuppertal in Germany, Moscow State University in Russia, the University of Manchester in the United Kingdom, and Boston University, Carnegie Mellon University, the Jet Propulsion Laboratory and Purdue University in the United States, pursued the fundamental and applied aspects of Bloch line memory, also known as micromagnetic memory. Beginning in 1986 at LETI in Grenoble, France, there were micromagnetic memory workshops at which researchers met to discuss their latest progress. Numerous papers on micromagnetic memory were presented at the Intermag and Magnetism and Magnetic Materials conferences. The corresponding manuscripts were published in the *IEEE Transactions on Magnetics* and the *Journal of Applied Physics.* In contrast to magnetic bubble memories, in which commercial products appeared within a decade of concept announcement, only small prototypes of VBL memory were ever achieved. With the technical difficulty inherent in achieving the micromagnetic memory and the fierce competition from competing technologies, work on Bloch line memory has been essentially abandoned.

MAGNETIC BUBBLE MEMORY

Overview

The magnetic bubble is the unit of information storage in a magnetic bubble memory. It is a cylindrical magnetic domain that resides in a thin film or platelet of magnetic material. The magnetization is oriented normal to the surface. An essential feature of a bubble material is a uniaxial anisotropy that maintains this magnetization orientation. The first bubble materials were thin platelets of orthoferrite in which bubbles, typically tens of microns in diameter, can be created. The orthoferrites soon gave way to thin films of magnetic garnet epitaxially grown on single crystal substrates of gadolinium gallium garnet (GGG). The garnet films supported bubbles with diameters orders of magnitude smaller, potentially less than 0.5 μm, and thus would enable higher storage densities. The general composition of the garnet is $RE_3Fe_5O_{12}$. The garnet films are prepared by liquid phase epitaxy. The GGG substrate is immersed into a platinum crucible containing a super-cooled melt of iron oxide, rare earth oxides and lead oxide, and the garnet film grows on the GGG. The uniaxial magnetic anisotropy is due to the way in which rare earth ions of different sizes become arranged in the crystal lattice; this is termed *growth-induced* anisotropy. By making appropriate substitutions on the rare earth (RE) and iron (Fe) sublattices, it is possible to prepare films with a wide range of magnetic and optical parameters.

Crystalline films of hexaferrites and amorphous films containing transition metals and rare earths, e.g. GdCo, can also support magnetic bubbles. An advantage of these materials is that the bubbles can have diameters smaller than the approximately 0.5 μm minimum diameter available in the garnet films. These materials thus offered the promise of very high-density bubble memory. However, because of technical and economic obstacles, commercial bubble memories were never produced with these materials.

Magnetic bubbles may be observed by means of the Faraday magneto-optic effect, in which the plane of polarized light is rotated by passage through a magnetic material. The bubble garnet films, with typical thickness of a few μm, exhibit on the order of 1° of Faraday rotation, which is sufficient for seeing the domains. This easy visual observation of the bubble domains was instrumental in research on magnetic bubbles.

Figure 2 shows a package for a bubble memory device. The outer and inner coils produce a rotating magnetic field in the plane of the film for propagating the bubbles, and a permanent magnet produces a magnetic field to maintain stable bubbles.

The typical bubble memory has a major-loop/minor-loop architecture as depicted in Fig. 3. The bubbles are stored in the minor loops. The positions in the loops are either empty or contain a bubble, depending on the state of that bit. Additional bubbles are used for error correction.

On the bubble chip is an overlay pattern of magnetic elements made from an alloy approximately 81% nickel and 19% iron, known as Permalloy. The bubbles are moved along the

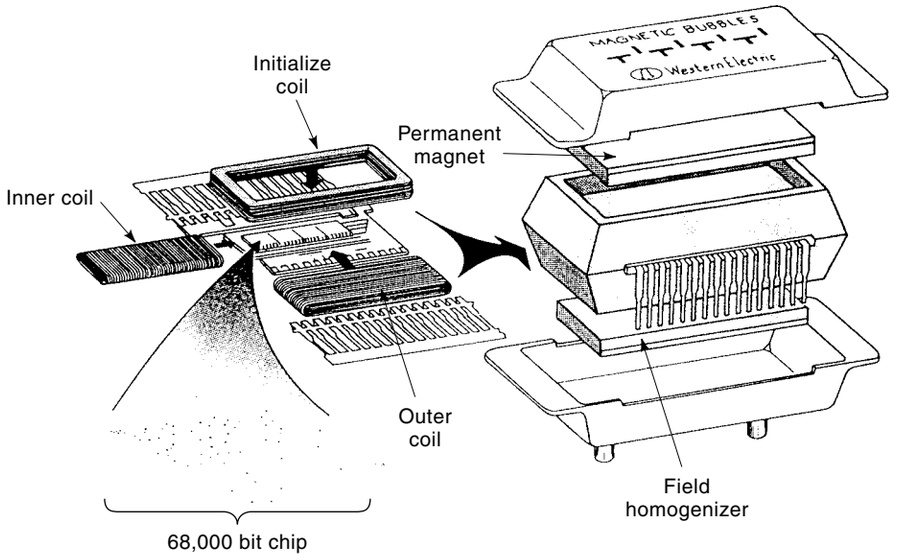

Figure 2. Package for a bubble memory device. (After A. H. Bobeck, I. Danylchuk, *IEEE Trans. Magn.* **MAG-13**, 1370–1372, 1977; © IEEE, 1977.)

loop by the interaction of the rotating in-plane magnetic field with the permalloy guiding elements. The process is illustrated in Fig. 4. The external in-plane magnetic field H_{ip} results in magnetic poles on the Permalloy elements, and the stray magnetic field from these poles moves the bubbles.

For reading or writing, bubbles are transferred between the minor loops and the major loops by swap gates. For reading, the bubble is replicated and transferred to a detector, which generally is a Permalloy thin film whose resistance is changed by the presence of the bubble. Writing is achieved by creating bubbles with a generator, often with a seed bubble. Erasure is achieved by failing to replicate the bubble as it travels through the major loop. In a bubble memory a representative frequency of the rotating magnetic field is about 100

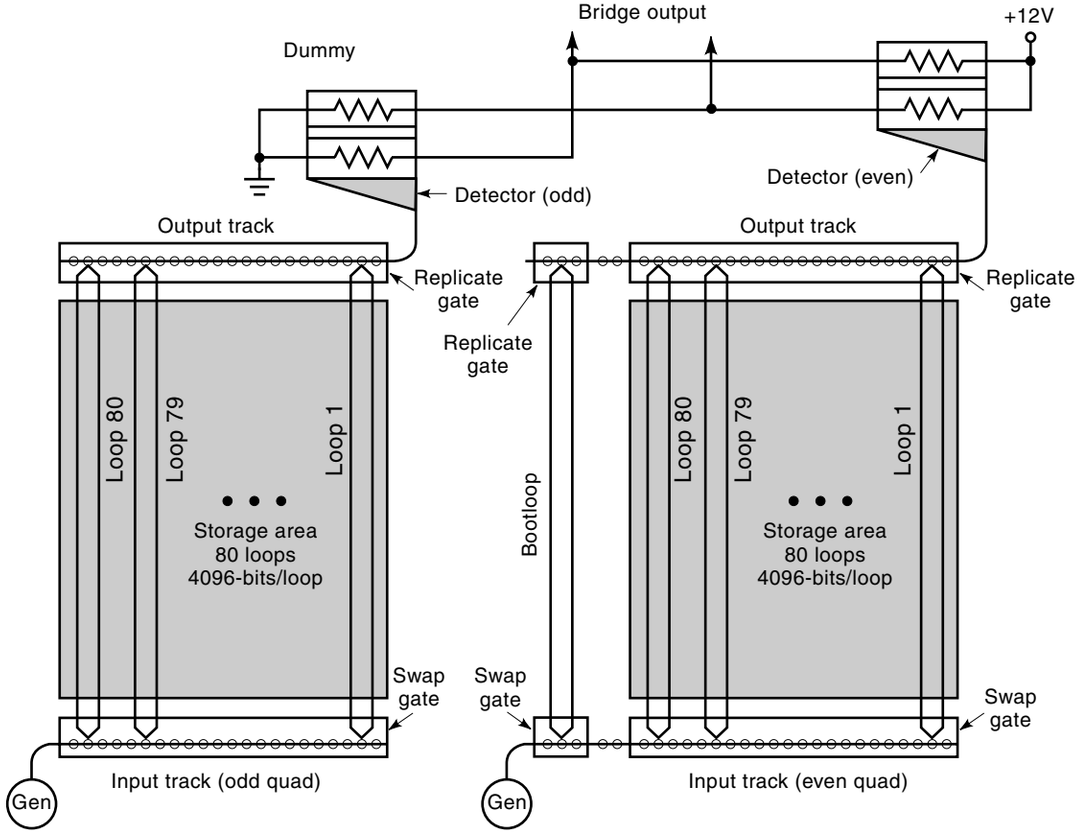

Figure 3. Bubble chip architecture. (Reprinted by permission of Intel Corporation; © Intel Corporation, 1995.)

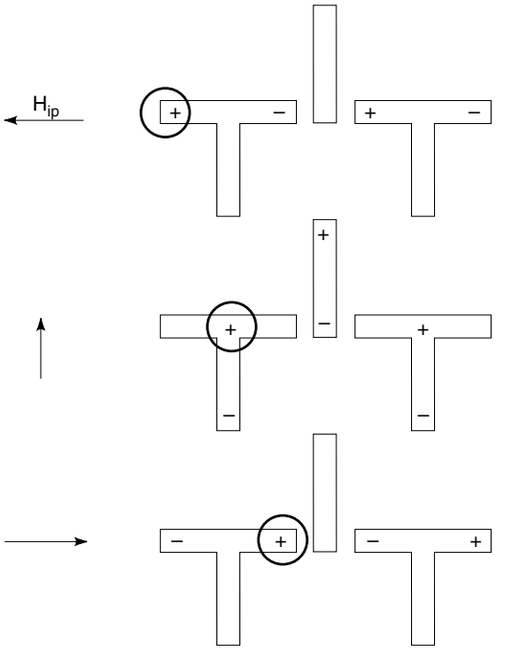

Figure 4. Permalloy pattern for movement of magnetic bubbles by an external magnetic field H_{ip}.

kHz and some 4000 bubbles are stored in a loop. Considering the time required to move the bubbles out of the minor loops and to the detector results in an average access time of about 20 ms.

Other shapes of propagation elements were used in addition to the TI bars discussed here. The C bar elements are shaped like the letter "C" and offer a greater storage density than the TI bars for a given minimum feature size in the photolithography. The asymmetric half disks have a shape which resembles a half-moon and also yield a greater storage density. An even greater storage density was promised by using overlapping disks, known as contiguous disks, as the guiding structures for the bubbles.

Domain Statics

In the demagnetized state, the domain pattern in a garnet film has the form of stripes, with magnetization pointing in opposite directions perpendicular to the plane of the film. Application of a perpendicular bias field reduces the width of stripes whose magnetization is antiparallel to the field, eventually converting the stripes to bubbles (Fig. 5). For a sufficiently large bias field, the bubbles collapse, and the entire film is uniformly magnetized.

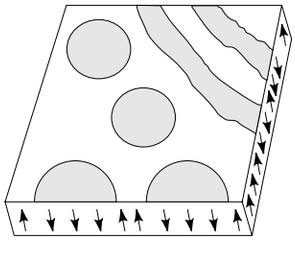

Figure 5. Stripe and bubble domains in a garnet film.

In the presence of an applied field $\boldsymbol{H}_a$, the micromagnetic energy $\boldsymbol{W}_m$ for a magnetic garnet layer is given by

$$W_m = -\int \boldsymbol{M}_s \cdot \boldsymbol{H}_a \, dV - \frac{1}{2}\int \boldsymbol{M}_s \cdot \boldsymbol{H}_d \, dV + A\int \left(\frac{\nabla \boldsymbol{M}_s}{M_s}\right)^2 dV + \int K_u \sin^2\theta \, dV \tag{1}$$

where $\boldsymbol{M}_s$ is the magnetization vector; $\boldsymbol{H}_d$ is the demagnetizing field which arises from the magnetic charges at the surface and in the domain walls; A is the exchange constant arising from the atomic forces which align the magnetization; K_u is the uniaxial anisotropic constant, and θ is the angle of magnetization with respect to the film normal. The integrals are evaluated over the volume V of the film. The magneto-elastic energy is usually not a significant factor in bubble garnets and is not included in Eq. (1). Also not included in Eq. (1) is the in-plane anisotropy energy, which is usually not a significant factor in (111)-oriented garnet films which are used in bubble memories. However, garnet films with other orientations, such as (110), can have a significant in-plane anisotropy.

For the easy direction of the magnetization to be normal to the film, it is necessary that the anisotropy energy density exceed the demagnetizing energy. This is expressed through the dimensionless Q factor:

$$Q = \frac{K_u}{2\pi M_s^2} \tag{2}$$

For perpendicular magnetization, Q must exceed unity, and for typical garnet bubble materials, $2 \lesssim Q \lesssim 10$.

The external bias field creates a force which shrinks the bubble, and the demagnetizing field expands it. Thiele (7) calculated the energy of the bubble in an external field as a function of the diameter. The stable bubble diameter is the diameter at which the energy is minimized. The lack of an energy minimum for any bubble diameter indicates that the external field either collapses the bubble or causes it to run out (into a stripe domain). The equation describing the equilibrium diameter of the bubble is

$$\frac{l}{h} + \frac{H_z}{4\pi M_s} \cdot \frac{d}{h} = F\left(\frac{d}{h}\right) \tag{3}$$

where

$$l = \frac{\sqrt{AK_u}}{\pi M_s^2} \tag{4}$$

is a parameter with dimensions of length, h is the thickness of the film, H_z is the external bias field and $F(d/h)$ is called the Thiele force function.

The collapse and runout diameters, d_{co} and d_{so}, respectively, are determined by the stability functions S_0 and S_2:

$$\frac{l}{h} = S_0\left(\frac{d_{co}}{h}\right) = S_2\left(\frac{d_{so}}{h}\right) \tag{5}$$

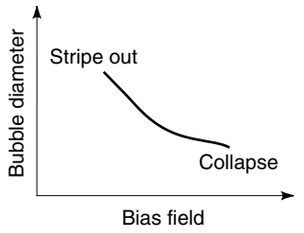

Figure 6. Graph of bubble diameter versus bias field.

Figure 6 schematically illustrates the dependence of bubble diameter on the external bias field and on the run out and collapse fields. For a typical garnet, the external field midway between collapse and stripeout fields, H_{co} and H_{so}, respectively, is about $0.3 \times 4\pi M_s$ and the difference between H_{co} and H_{so} is about $0.1 \times 4\pi M_s$. Thus, a representative garnet field with magnetization of $4\pi M_s = 400$ G has representative values of collapse and stripeout fields of approximately 140 and 100 G, respectively.

The magnetic domain wall is the transition region over which the magnetization changes direction by π radians between the inside and outside of the bubble. (By convention, the magnetization outside the bubble is in the z-direction.) In a simplified model, the spin distribution in the wall is caused by the exchange energy, which favors a wider wall, and the anisotropy energy, which favors a narrower wall. Consider a one-dimensional wall depicted in Fig. 7 with variation in the y-direction and with the zero of the y-coordinate at the wall center. The total energy σ_w per unit width and thickness of domain wall is given by

$$\sigma_w = \int_{-\infty}^{\infty} \left[K_u \sin^2 \theta + A \left(\frac{\partial \theta}{\partial y} \right)^2 \right] dy \tag{6}$$

where θ is the angle of the magnetization with respect to the film normal. Utilizing the calculus of variations to minimize the energy results in the domain wall profile,

$$\tan \frac{\theta}{2} = \exp \left(y \sqrt{\frac{K_u}{A}} \right) \tag{7}$$

Application of Eq. (7) to Eq. (6) results in $\sigma_w = 4\sqrt{AK_u}$.

At the midpoint of the wall, $d\theta/dy = \sqrt{K_u/A}$. The wall width parameter δ_w is the wall which would arise assuming the spin gradient were constant:

$$\delta_w = \frac{\pi}{\left. \frac{d\theta}{dy} \right|_{y=0}} = \pi \sqrt{\frac{A}{K_u}} \tag{8}$$

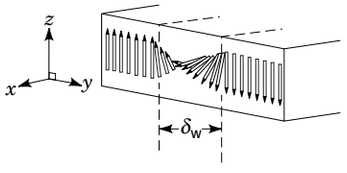

Figure 7. Magnetic domain wall in a bubble garnet film. The spin orientation changes by nearly 180° over a width of δ_w.

Magnetic Bubble Dynamics. A straight magnetic domain wall in the presence of a perpendicular magnetic field H_z experiences a normal force per unit area f_n given by

$$f_n = -\frac{\partial w_m}{\partial y} = -\frac{\partial}{\partial y}(-2M_s H_z y) = 2MH_z \tag{9}$$

where w_m is the magnetostatic energy density and y is the displacement normal to the wall. In response to this force, the magnetic spins in the wall are displaced and the wall moves. The wall motion is described by

$$f_n - 2M_s H_c = \frac{2M_s}{\mu} v_n \tag{10}$$

where v_n is the normal wall velocity, H_c is the coercive field, or simply coercivity, and μ is the wall mobility. Combining Eqs. (9) and (10) results in the linear mobility relationship

$$v_n = \mu(H_z - H_c) \tag{11}$$

The domain wall moves in the response to the applied field so that the viscous force acting on the moving wall equals the force of the applied field. The mobility is given by

$$\mu = \frac{\gamma \delta_W}{\pi \alpha} \tag{12}$$

where γ is the gyromagnetic constant and α is the dimensionless damping parameter.

A magnetic bubble moves in response to a gradient in bias field $\nabla \boldsymbol{H}_z$. Using Eq. (9) and integrating the magnetic field around the domain wall yields

$$\boldsymbol{f}_n = \pi M_s h r (2r \nabla \boldsymbol{H}_z) \tag{13}$$

where r is the bubble radius.

Integrating the force in Eq. (10) required to move a straight wall around the wall of the bubble results in the force f required to move the bubble at speed V:

$$f = \frac{2\pi M_s h r V}{\mu} + 8M_s h r H_c \tag{14}$$

Combining Eqs. (13) and (14) results in the velocity versus drive field relationship for a bubble moving in the y-direction:

$$V_y = \frac{\mu}{2} \left(2r \frac{\partial H_z}{\partial y} - \frac{8}{\pi} H_c \right) \tag{15}$$

where r is the bubble radius. Equation (15) does not account for the force due to the magnetic structure in the domain wall. This additional force is discussed in the next section.

Domain Wall Structure

A rich variety of structure is possible in the wall of the magnetic bubble. In Fig. 7, an ideal 180° Bloch wall (separating domains pointing in opposite directions) is shown. If the magnetization rotates in the plane of the spins on either side of the wall, the resulting structure is called a Néel wall. Actual wall structures are more complicated, largely due to the effects of the demagnetizing fields.

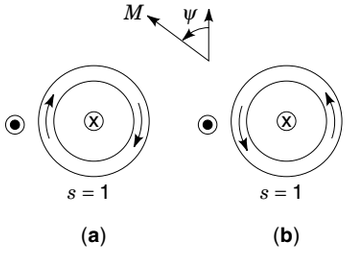

Figure 8. The two possible unichiral bubble states. The angle ψ is the direction of the magnetization with respect to a fixed direction in the plane of the film. The arrows represent the direction of the magnetic spins at the middle of the domain wall.

The magnetic spins rotate clockwise or counterclockwise through the wall, resulting in center of wall spins directed in either the clockwise or counterclockwise directions. The winding number S is the number of 2π revolutions made by the midwall magnetization in the counterclockwise direction around the circumference of the bubble:

$$S = \frac{1}{2\pi h} \int d\psi \int_0^h dz \tag{16}$$

where ψ is the angle made by the magnetization with a fixed direction in the film plane.

Two bubbles are shown in Fig. 8. The bubble in Fig. 8(a) has midwall spins directed in the clockwise direction and the bubble in Fig. 8(b) has the spins in the counterclockwise direction. However, traversing the entire circumference of bubble, the total spin rotation in both cases is $+2\pi$ radians. Such a bubble is called a unichiral bubble with $S = 1$. However, additional structure can occur, resulting in transitional regions between wall segments, called Bloch lines, as shown in Fig. 9. Across the vertical Bloch line, which spans the film thickness, the magnetic spins change direction by π radians. Figure 9 shows three bubbles with two Bloch lines each. The winding number depends on the rotation sense of the Bloch lines. A positive Bloch line has a rotation of $+\pi$ radians and a negative Bloch line has a rotation of $-\pi$ radians. Figure 9(a) shows a bubble where $S = 1$. The Bloch line on top is negative and has a rotation of $-\pi$ radians. The Bloch line on the botton has a rotation of $+\pi$ radians. The twist angles of the two Bloch lines cancel and the bubble has winding number of $S = 1$, the same as the states depicted in Fig. 8. In Fig. 9(b) both of the Bloch lines have a twist of $-\pi$ radians and the winding number $S = 0$. In Fig. 9(c), the twists of both Bloch lines are $+\pi$ radians and $S = 2$.

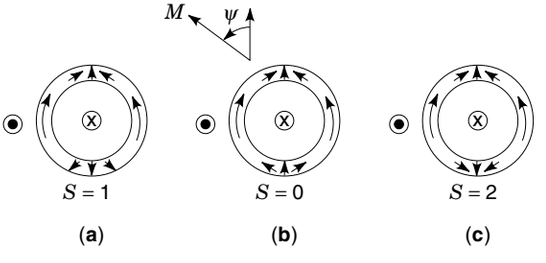

Figure 9. Three bubble states with two vertical Bloch lines.

In general, for a bubble with Bloch lines which span the film thickness, the winding S is given by

$$S = 1 + \frac{1}{2}(n_+ - n_-) \tag{17}$$

where n_+ and n_- are the number of positive and negative VBLs, respectively.

Horizontal Bloch lines do not penetrate the entire thickness of the bubble. Their influence on bubble motion is not fully understood.

The magnetic force, defined in Eq. (13), that is required to move a bubble depends on the domain wall structure. In addition to the viscous damping force acting parallel to the velocity of the moving bubble, there is also a force F_x that acts on the bubble transverse to the velocity. This additional force that deflects the bubble from its "straight line" motion from the gradient field is caused by the wall structure of the moving bubble.

The transverse force is caused by twists of magnetization in the domain wall described previously, and for a bubble moving in the y direction is given by

$$F_x = \pi Mhr\left(2r\frac{\partial H_z}{\partial x}\right) = \frac{4\pi MSh}{\gamma} V_y \tag{18}$$

where S is the winding number described before. The transverse force on the bubble, known as the gyrotropic force, results in a deflection angle between the direction of the applied gradient and the velocity.

Malozemoff and Maekawa (8) described how Bloch line structure is generated when the bubble is moved at sufficiently high translational velocity. A consequence of dynamic conversion is that there is a maximum velocity, the saturation velocity, at which the bubble can be moved, no matter how large the drive field is. The saturation velocity is approximately equal to the velocity at which Bloch line structures are dynamically generated.

There is some debate regarding the detailed mechanism of dynamic conversion. Thiele (9) has postulated that wall-bound spin waves lead to the formation of Bloch lines. In the Bloch curve model (10) it is postulated that there is a layer of in-plane magnetization on each surface of the bubble film. These layers result from the strong demagnetizing fields near the film surfaces. At these "critical circles," Bloch curves, across which the mid-wall magnetization changes direction, are nucleated. The shape of the Bloch curve arises from the two competing forces which act on it. The gyrotropic force expands the Bloch curve, and the line tension force contracts it. Once a critical velocity is reached at $0.6V_p$, where $V_p = 24.9\gamma A/h\sqrt{K_u}$, the gyrotropic force dominates, and the Bloch curve expands. The shape of the curve for a given velocity will be determined by the combination of gyrotropic force and line tension. At a bubble translation velocity of V_p, the Bloch curve reaches the critical circle on the opposite side of the film. Then the Bloch curve either "punches through" into two vertical Bloch lines or does not punch through and "stacks." These two processes are illustrated in Fig. 10.

The rotating gradient method (11) is an experimental technique that demonstrates the dynamic generation of VBLs. The apparatus is depicted in Fig. 11. Currents pass through four drive conductors to create a rotating gradient field that

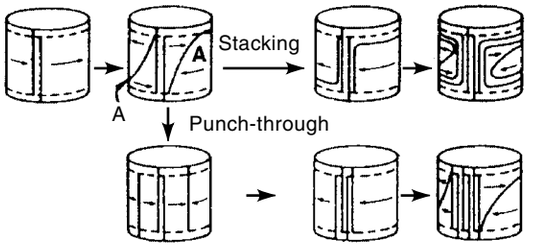

Figure 10. The dynamic generation of Bloch line structure in a magnetic bubble. (After Ref. 8; © AIP, 1976.)

maintains the bubble in a steady-state circular motion. A radial restoring force also brings the bubble to the center of the conductor array. The trajectory of the bubble is magneto-optically observed. The components of magnetic force acting on the moving bubble may be determined from the phase angle ϕ. The radial magnetic field that acts on the bubble perpendicular to the velocity yields information on the number and type of Bloch lines. The equation of motion for the rotating gradient experiment is

$$h_r = 2r\nabla H_r = \frac{\xi 4SV}{\gamma r} + \frac{2\omega}{\gamma} p \tag{19}$$

where ∇H_r is the gradient in H_z in a direction perpendicular to the velocity, $\xi = +1$ or -1 for clockwise or counterclockwise rotation, respectively, ω is the rotational rate, and p is the dimensionless momentum. For a bubble with vertical Bloch lines,

$$p = n_+ + n_- \tag{20}$$

The number and type of VBLs in the moving bubble may be determined from the measurement of dimensionless momentum. Figure 12 shows bubble velocity V versus p for five states in a rotating gradient experiment, convincingly showing the presence of VBLs. The peak velocity of the different states is limited by the creation of VBL structures.

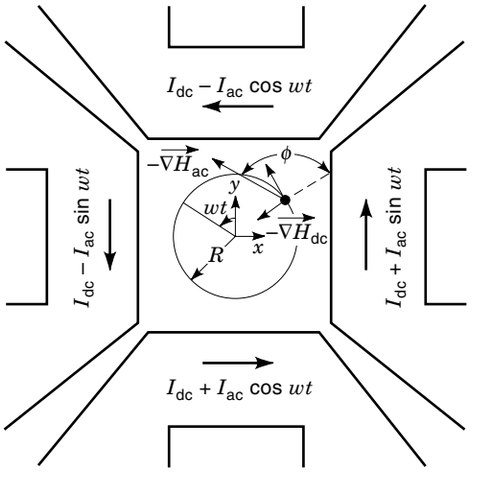

Figure 11. Rotating gradient apparatus. (After Ref. 11.)

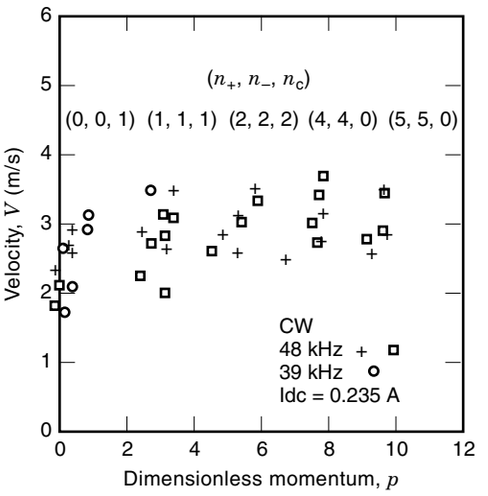

Figure 12. Velocity versus dimensionless momentum observed in a rotating gradient experiment for five states of a magnetic bubble. The number of positive VBLs, negative VBLs and Bloch curves respectively are represented by (n_+, n_-, n_c). (After Ref. 11.)

BLOCH LINE MEMORY

In a Bloch line memory (6,12), information is stored in VBLs arranged along stripe domains. The principal concepts are illustrated in Figs. 13 and 14. To read information, a magnetic stripe domain is expanded under a pair of conductors. A pulse of current is passed through the pair of conductors which produces a perpendicular magnetic field between the conductors. With a VBL at the head of the stripe, the stripe is chopped by the bias pulse, and a bubble is created. The readout is nondestructive because the original VBL in the head of the stripe is replicated. If the head of the stripe does not contain a vertical Bloch line, the stripe is not chopped by the pulse,

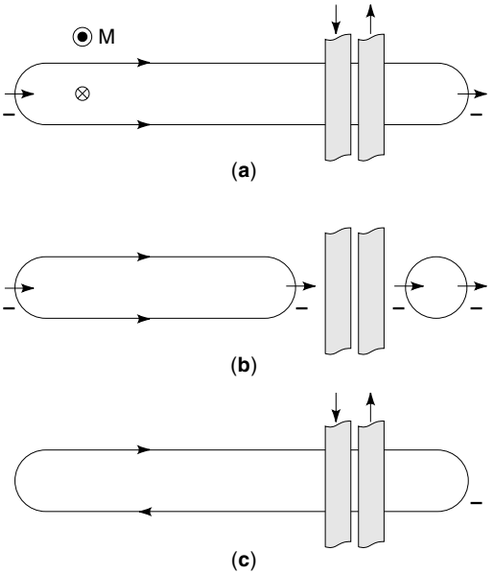

Figure 13. Reading of information in a Bloch line memory by stripe chopping. (After Ref. 6; © IEEE, 1983.)

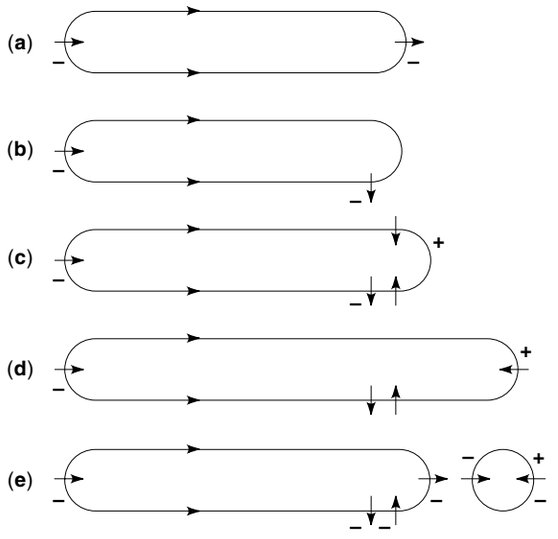

Figure 14. Writing of information in a Bloch line memory by addition of a negative VBL pair to a stripe domain. (After Ref. 6; © IEEE, 1983.)

and no bubble is produced. The presence or absence of a bubble after the chopping process is detected by the same type of detector which is used in a bubble memory.

For the writing process, illustrated in Fig. 14, a negative VBL is brought to the end of the stripe, and a local bias field pulse is applied to generate a pair of opposite twist VBLs. The positive VBL is left at the end of the stripe, and the negative one is brought away. Then a chopping pulse is used to cut off the head of the stripe, and a negative VBL is formed at the end of the remaining stripe.

VBL memory offered the theoretical possibility of a very high density of information. The spacing between Bloch lines was estimated to be equal to the Bloch line width parameter $2\pi\Lambda$, where

$$\Lambda = \sqrt{\frac{A}{2\pi M_s^2}} \tag{21}$$

For a garnet supporting 0.5 μm stripes, approximately the minimum attainable in garnet materials, the estimated density was 1.6 Gbit/cm^2. This density was a significant increase over that attainable for bubble memory, and there was the promise of a revival of solid-state magnetic memory.

The midwall spins along the length of a VBL usually all point in the same direction. If the VBL contains a Bloch point, the midwall spins on either side of the Bloch point point in opposite directions. The nucleation of a point at either film surface could change the polarity of a VBL. Then this converted Bloch line and a neighboring one would mutually annihilate, resulting in information loss. Thus an important theoretical estimate for the reliability of information storage in a Bloch line memory is the the energy required to nucleate a Bloch point. The energy W_{bp} required to create a Bloch point is given by

$$W_{bp} = 2\pi A^{3/2}\sqrt{K}(\ln Q + 1.9) \tag{22}$$

Using values for a garnet with 0.5 μm stripewidth, W_{bp} was calculated to be approximately 3×10^{-11} erg, well in excess of the thermal energy kT, which is about 4.2×10^{-14} erg at room temperature. Thus thermally nucleated Bloch points were not expected to pose a reliability problem for Bloch line memory.

Progress in bubble memories was rapid after the technological concept was announced. This was caused in large part by the fact that the bubbles could be magneto-optically observed, providing rapid feedback on the efficacy of engineering modifications. Vertical Bloch lines are much more difficult to visualize magneto-optically. The Bloch lines can not be seen in a normal microscope used to see magnetic bubbles. An important development in Bloch line technology was the development of polarized anisotropic dark-field observation (PADO) by Thiaville and collaborators (13). The Bloch lines were visualized with a laser scanning microscope with polarization analysis. A simpler technique for observing VBLs was developed by Theile and Engemann (14). A prism is used to refract the light incident on the garnet sample so the VBLs are detected by dark-field illumination.

The marriage between the bubble technology required to read and write VBLs and a stripe structure in which VBLs could be reliably propagated never reached a successful conclusion. For economic reasons, including problems of inadequate predicted yield due to small margins in a number of essential parameters and greater densities and lower costs in the competing technologies of semiconductor memories and magnetic disk drives, VBL development has essentially come to a halt at this point.

BIBLIOGRAPHY

1. C. Kooy and U. Enz, Experimental and theoretical study of the domain configuration in thin layers of $BaFe_{12}O_{19}$, *Philips Res. Rep.,* **15**: 7–29, 1960.
2. A. H. Bobeck, Properties and device applications of magnetic domains in orthoferrites, *Bell Syst. Tech. J.,* **46**: 1901–1925, 1967.
3. H. Chang, *Magnetic Bubble Memory Technology,* New York: Marcel Dekker, 1978.
4. E. Feldtkeller, Mikromagnetisch stetige und unstetige Magnetisierungskonfigurationen, *Zeitschrift fuer Angewandte Physik,* **19**: 530, 1965.
5. A.P. Malozemoff and J. C. Slonczewski, *Magnetic Domain Walls in Bubble Materials,* New York: Academic Press, 1979.
6. S. Konishi, A new ultra-high density solid state memory: Bloch line memory, *IEEE Trans. Magn.,* **MAG-19**: 1838, 1983.
7. A. A. Thiele, *Bell Syst. Tech. J.,* **48**: 3287–3335, 1969.
8. A. P. Malozemoff and S. Maekawa, Detection of stored momentum in magnetic bubbles by a bias jump effect, *J. Appl. Phys.,* **47**: 3321–3328, 1976.
9. A. A. Thiele, Applications of the gyrocoupling vector and dissipation dyadic in the dynamics of magnetic domains, *J. Appl. Phys.,* **45**: 377–393, 1974.
10. A. P. Malozemoff, J. C. Slonczewski, and J. C. DeLuca, Translational velocities and ballistic overshoot of bubbles in garnet films, *AIP Conf. Proc.,* **29**: 58, 1976.
11. J. A. Nyenhuis, F. J. Friedlaender, and H. Sato, Wall states of a bubble in a rotating field gradient, *IEEE Trans. Magn.,* **MAG-19**: 1796–1801, 1983.
12. F. B. Humphrey and J. C. Wu, Vertical Bloch line memory, *IEEE Trans. Magn.,* **MAG-21**: 1762–1766, 1985.

13. A. Thiaville et al., Direct Bloch line optical observation, *J. Appl. Phys.,* **63**: 3153–3158, 1988.

14. J. Theile and J. Engemann, Direct optical observation of Bloch lines and their motion in uniaxial garnet films using a polarizing light microscope, *Appl. Phys. Lett.,* **53**: 713–715, 1988.

Reading List

A. H. Bobeck and E. Della Torre, *Magnetic Bubbles,* North Holland, 1975.

A. H. Bobeck and H. E. D. Scovil, Magnetic bubbles, *Scientific American,* **224** (6): 78–90, 1971.

H. Chang, *Magnetic Bubble Technology,* New York: IEEE Press/Wiley, 1975.

A. H. Eschenfelder, *Magnetic Bubble Technology,* New York: Marcel Dekker, 1978.

Magnetic Bubbles, *Proc. Winter School New Magn. Mater.,* Warsaw: Polish Scientific Publishers, 1976.

A. P. Malozemoff and J. C. Slonczewski, *Magnetic Domains Walls in Bubble Material,* New York: Academic Press, 1979.

T. H. O'Dell, *Magnetic Bubbles,* New York: Wiley, 1974.

G. Winkler, *Magnetic Garnets,* Braunschweig, Germany: Vieweg, 1981.

F. J. FRIEDLAENDER
J. A. NYENHUIS
Purdue University